ECS Journal of Solid State
Science and Technology

Morphological and Electrical Properties of Polythiophene Nanostructured Film Synthesized Using Atmospheric Pressure-Plasma Reactor with Double V-Shaped Bare Electrode

ECS Journal of Solid State Science and Technology, 2022 **11** 064005
2162-8777/2022/11(6)/064005/9/$40.00 © 2022 The Electrochemical Society ("ECS"). Published on behalf of ECS by IOP Publishing Limited

Morphological and Electrical Properties of Polythiophene Nanostructured Film Synthesized Using Atmospheric Pressure-Plasma Reactor with Double V-Shaped Bare Electrode

Habeeb Olaitan Suleiman,[1,=] Jae Young Kim,[1,=] Hyo Jun Jang,[1] Eun Young Jung,[1] Muhan Choi,[1,2,3] and Heung-Sik Tae[1,2,z]

[1]*School of Electronic and Electrical Engineering, College of IT Engineering, Kyungpook National University, Daegu 41566, Republic of Korea*
[2]*School of Electronics Engineering, College of IT Engineering, Kyungpook National University, Daegu 41566, Republic of Korea*
[3]*Digital Technology Research Center, Kyungpook National University, Daegu 41566, Republic of Korea*

To synthesize a wide-area conducting polymer with improved morphology and electrical properties, we proposed a new atmospheric pressure (AP) plasma reactor with double V-shaped bare wire electrode operating at a low driven voltage to expand the plasma area for nanostructure synthesis. The two wires form a V-shape making a 60° angle at the edges and are joined together forming a cross, creating a canopy-like plasma medium in the plasma reactor center. Using the AP-plasma reactor, the polythiophene (PTh) nanostructured films are successfully synthesized with and without iodine doping. Moreover, the molecular structures and chemical properties of nascent and iodine-doped PTh films are compared, and the electrical resistivities of ex situ and in situ iodine-doped PTh nanostructures are also analyzed.
 [DOI: 10.1149/2162-8777/ac7660]

Manuscript submitted February 21, 2022; revised manuscript received May 24, 2022. Published June 20, 2022.

Supplementary material for this article is available online

Atmospheric pressure (AP)-plasma polymerization uses a non-thermal gaseous discharge to synthesize polymer composites at AP. Ionization and excitation of gas particles by electric discharge create reactive species of precursor particles to crosslink them without raising the temperature.[1–4] The AP-plasma polymerization provides good adhesion of the synthesized material to the substrates of various surface properties, offering an alternative to expensive vacuum systems.[5–8] Since high-electron-energy profile and various reactive species attained at low gaseous temperature enable a nanostructured thin film to be deposited on a complex, AP-plasma can be used to synthesize conjugated polymers.[9–11] In fabricating conductive polymer films, the AP plasma polymerization method has the great advantage of a simple process compared to electrochemical polymerization, which has a multi-step method of synthesizing conjugated polymer particles, depositing them as a film, and functionalizing it with electrical properties. In particular, in situ halogen doping is an in-line functionalization method that can be readily combined to plasma polymerization in which nucleation and crosslinking reactions occur in the gas phase.

Conjugated polymers, including polyaniline, polypyrrole, and polythiophene generally exhibit a conductivity, ranging from insulators to metallic behavior.[12,13] They comprise backbone chains of localized π-electrons alternating between single and double bonds. [14] Thus, conjugated polymers conduct electricity by delocalizing π-electrons through oxidation or reduction, providing them with state-of-the-art materials for the next-generation electronic and optical devices.[15,16] Polythiophene (PTh) is one of the most promising conductive polymers due to its environmental stability, high charge carrier mobility, and extended absorption wavelength.[14] Owing to these properties, PTh and its derivatives find many applications in electronic devices, such as electrodes of polymer light emitting diodes, gas sensors, organic field effect transistors, actuators, electrochromic displays and supercapacitors, gaining vast attention from several researchers.[12,17–20]

Recently, our research group reported the use of AP-plasma jet array with a guided tube and a bluff-body to maintain the uniformity of the mixture of argon (Ar) gas and precursor producing a nonthermal plasma for the synthesis of various polymers and copolymer of thiophene and aniline.[21–23] More recently, AP-plasma reactors with exposed pin electrodes in the reaction region have been used to control the structural properties of polymers by preventing excessive crosslinking through the reduced monomer reactivity.[24] The AP-plasma reactor with the pointed bare electrode did not require charging and discharging of the dielectric barrier, thus generating the plasma medium at a lower voltage. In addition, this enabled the supply of sublimated iodine (I_2) through the gas supply line, providing the electrical conductivity to the polymer.[15,24–26] However, since this AP-plasma reactor used a single pin-type electrode, it showed non-uniform deposition in the polymerization processing area despite the structural optimization efforts.

In this study, an AP-plasma reactor with crossed V electrodes is newly proposed to improve the structural and electrical properties of PTh nanostructured films and produce large-area PTh films with a surface area of several square centimeters. A stripped tungsten wire is used as a powered electrode operating at a low driven voltage to maintain the discharge for PTh synthesis. Experimental conditions are optimized to obtain a uniform and wide PTh film, and the morphological and chemical properties are analyzed, with and without I_2 doping. The electrical resistances of both ex situ and in situ I_2-doped PTh nanostructures are also analyzed.

Experimental

Experimental setup for AP-plasma polymerization.—Figure 1 shows a schematic diagram of the new AP-plasma reactor configuration and experimental steps for the synthesis of PTh nanostructured film. The AP-plasma reactor comprised a wide glass tube (guided tube) providing a plasma generating region and a nucleation region, a narrow glass tube supplying Ar gas containing a vaporized thiophene monomer to the nucleation area, a wire electrode covered with a glass capillary, and a cylindrical PTFE substrate stand, as shown in Fig. 1a. The guided tube was equipped with a 2 mm-diameter glass capillary with a 500 μm-diameter tungsten wire electrode, only the central 5-mm of the wire was exposed to the plasma reactor chamber (Fig. 1b). The tungsten wire electrode with a double V-shape makes a 60° angle at the center of the wide tube. Two V-shaped tungsten wires crossed at 90 degrees are used as the powered electrode. Since the shape of the electrode is horizontally a two-dimensional configuration, it is suitable for the formation of a wide nanostructured PTh film in the range of several square

=Equal Contribution.
zE-mail: hstae@ee.knu.ac.kr

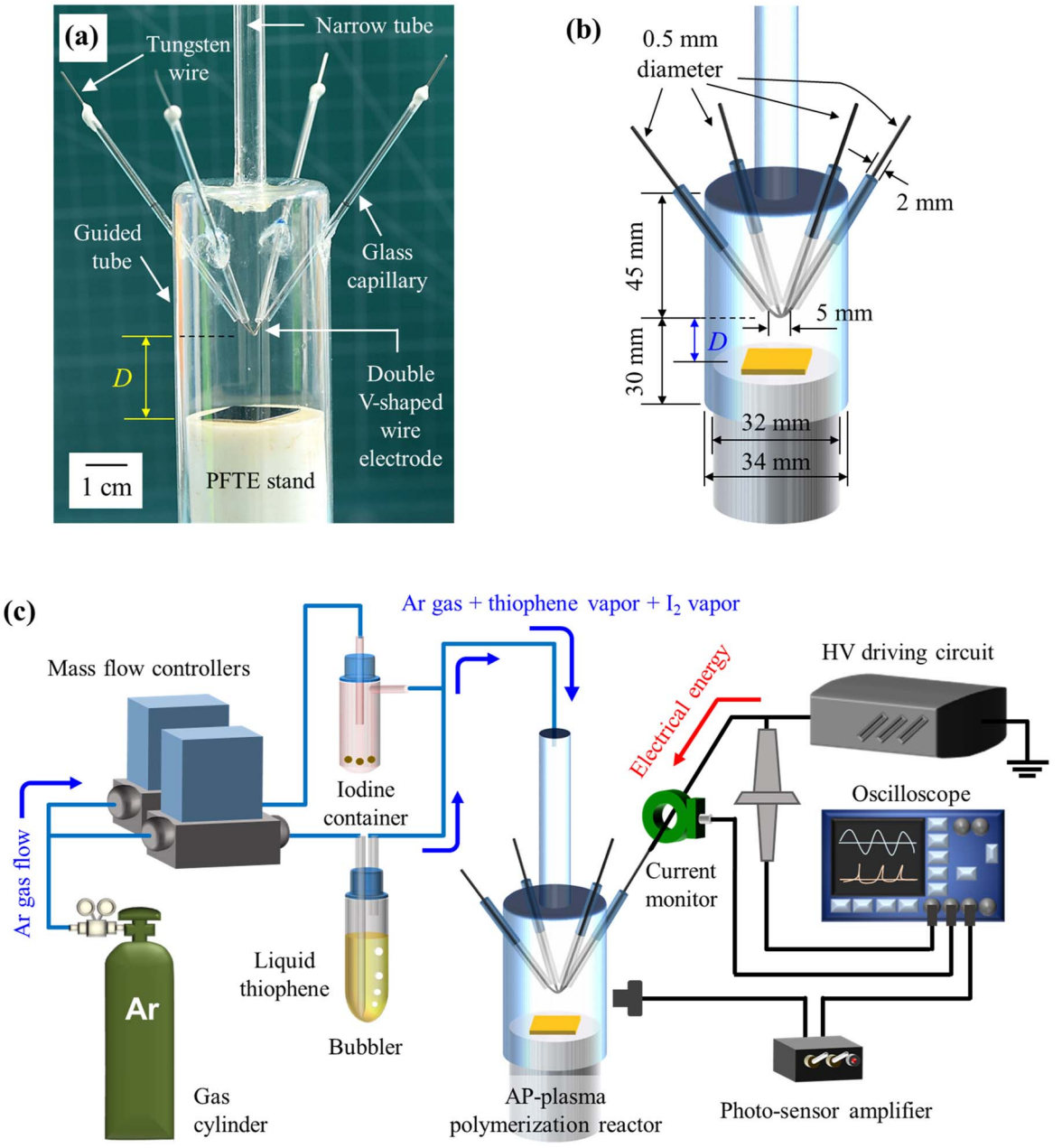

Figure 1. Experimental setup: (a) schematics of AP-plasma reactor with double V-shaped bare electrode, (b) photograph of AP-plasma reactor, and (c) schematic diagram of experimental setup including in situ iodine doping method.

centimeters compared to using a pin-pointed electrode. Ar gas emitted from the narrow gas-feeding tube in line with the center of the cylindrical PTFE stand collided with, and was reflected back by, the PTFE stand. Thus, the PTFE stand functioned as both a support for the substrate, and as a bluff body. In addition, the centered arrangement of the guided tube and PTFE stand allowed the discharge gas to leak through a gap of 1-mm from both sides of the guided tube to the PTFE stand, allowing the discharge gas to slowly exit the AP-plasma reactor.

To investigate the morphological and electrical properties of the PTh film by iodine (I_2) doping, pure PTh film, ex situ, and in situ I_2-doped PTh films were prepared, respectively. The schematic diagram of the entire experimental setup employed in the present study is shown in Fig. 1c. An HP-grade Ar gas with 99.999% purity was employed for the AP-plasma polymerization, and the gas supply line was split into two for the independent control of the Ar gas flow rates for the primary discharge gas and thiophene vapor. The primary Ar gas had a flow rate of 1500 standard cubic centimeters per minute (sccm), and a liquid thiophene monomer with a molecular weight of 84.14 $g \cdot mol^{-1}$ (Sigma-Aldrich Co., St. Louis, MO, USA) was vaporized using a glass bubbler supplying an Ar flow rate of 100 sccm.

For pure PTh films, PTh was deposited directly without iodine lines, while in situ I_2-doped PTh films used iodine lines for polymerization. For the in situ I_2 doping, a 50-ml glass bottle containing 3 g of iodine pellet (Daejung Chemical & Materials Corp., South Korea) was connected to the main Ar gas supply line. For the AP polymerization of nascent PTh film, the iodine bottle was simply removed from the system, as shown in Fig. 1c. Ex-situ I_2-doped PTh sample was prepared by vacuum-sealing a pure PTh sample with three iodine pellets (~40 mg) for 30 min. To test the electrical properties by I_2 doping, PTh nanostructured films were deposited on an interdigitated electrode (IDE)-patterned silicon (Si) substrate. The IDE had an interdigitated comb-shaped two-electrode

structure with 20 microelectrode pairs. The width of an IDE was 10.8 μm, with the spacing between the adjacent IDEs of 2.54 μm. Using an inverter-type driving circuit, a sinusoidal high-voltage with a peak value of 7 kV and a frequency of 28 kHz was applied to the powered electrode of the AP-plasma reactor. The experimental conditions for the AP-plasma polymerization are summarized in Table I.

Characterization of the gaseous discharge and analysis of the PTh nanostructured film.—To study the discharge behavior, a powered electrode was connected to a high-voltage probe (P6015A, Tektronix Inc., Beaverton, OR, USA), and a current probe (4100, Pearson Elec. Inc., Palo Alto, CA, USA) was connected to the wire electrode to observe the waveform with a digital oscilloscope (WaveRunner 64Xi, Teledyne LeCroy Inc., Chestnut Ridge, NY, USA). A photo-sensor amplifier (C6386–01, Hamamatsu Corp., Hamamatsu, Japan) was used to observe the wavelength-unresolved optical emission during the plasma polymerization.

To explore the creation of plasma in the reactor chamber, photographs of the AP-plasma reactor were obtained using a digital single-lens reflex camera (D5300, Nikon Corp., Tokyo, Japan) equipped with a Macro 1:1 lens (Tamron SP AF 90 mm F2.8 Di, Tamron Co., Ltd., Saitama, Japan). An intensified charge-coupled device (ICCD) camera (PI-MAX II, Princeton Instruments Inc., Trenton, NJ, USA) was used to identify the spatial distribution of the generated plasma. ICCD images were taken in the shutter mode with a gain of 10 and an exposure time of 1 μs.

The surface morphology, thickness, and vertical alignment of the PTh films on the Si substrates were monitored via a field emission scanning electron microscopy (FE-SEM) imaging (SU8220, Hitachi High-Technologies, Tokyo, Japan) with accelerated electrons at a 3-kV voltage and 10-μA current. The samples were coated with conductive platinum to avoid the surface charging problems during analysis.

A high-resolution transmission electron microscopy (TEM) images were obtained with a Titan G2 ChemiSTEM Cs Probe (FEI Company, Hillsboro, OR, USA) operating at 200 kV. The PTh nanoparticles for the TEM sample were prepared by depositing it in 10 μl DI water, ultrasonically dispersing onto carbon-coated copper grids and drying in air.

To characterize the functional groups and chemical composition of the deposited PTh films, we analyzed the films by using Fourier-transform infra-red (FT-IR) and X-ray photoelectron spectrometer (XPS) techniques. The molecular structures of the PTh films synthesized under different conditions were examined and compared via FTIR (Vertex 70, Bruker, Ettlingen, Germany) at the KBSI (Daegu, Korea). Attenuated total reflection Fourier-transform infra-red (ATR-FTIR) spectra were measured by averaging 128 scans in the range of 650–4000 cm^{-1} at a wavenumber resolution of 0.6 cm^{-1}.

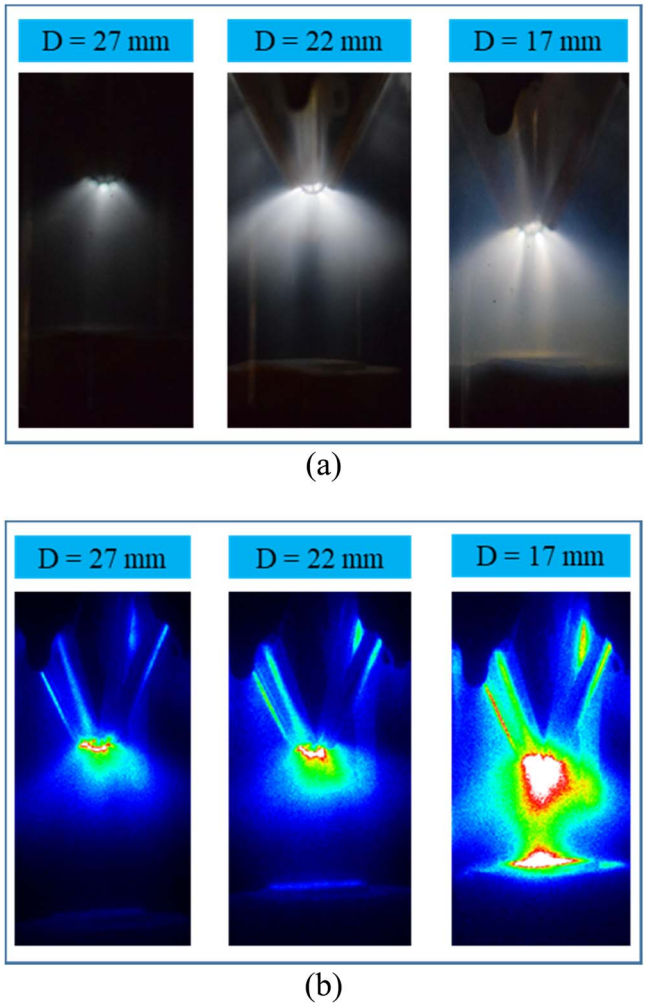

Figure 2. (a) Digital photographs and (b) intensified charge-coupled device (ICCD) images of plasma emission within the AP-plasma reactor.

The XPS was carried out on an ESCALAB 250XI surface analysis system (Thermo Fisher Scientific, Waltham, MA, USA), using monochromatic Al Kα X-ray source (hυ = 1486.71 eV) operated at 15 kV and 20 mA. The pressure in the analyzing chamber was

Table I. AP-plasma polymerization configuration and optimized experimental conditions.

	Experimental conditions	AP-plasma reactor
Device Configurations	Powered electrode shape	Double V
	Electrode material	Tungsten wire
	Electrode angle	60°
	Inner diameter of wide tube	34 mm
	Diameter of substrate stand	32 mm
	Distance between electrode and substrate	17 mm, 22 mm, 27 mm
Driving Conditions	Voltage waveform	Sinusoidal
	Plasma initiation voltage (V_p)	4 kV
	Plasma driving voltage (V_p)	7 kV
	Driving frequency	28 kHz
Gas Conditions	Discharge and monomer carrier gas	Ar (HP-grade: 99.999%)
	Gas flow rate for AP-plasma discharge	1500 sccm
	Gas flow rate for thiophene vapor	100 sccm
	Polymerization process time	10 min

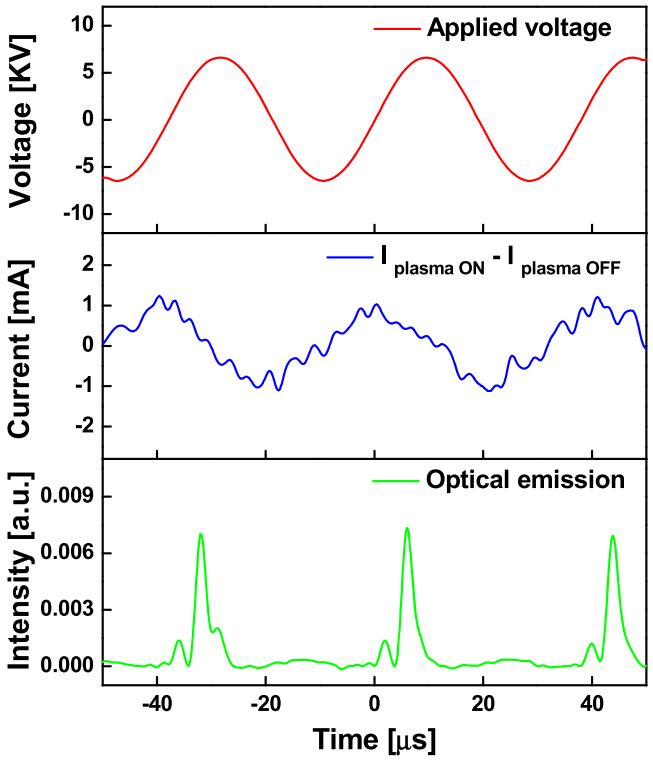

Figure 3. Instantaneous behavior of the driving voltage, discharge current, and optical emission from the proposed AP-plasma reactor during polymerization.

maintained at 10^{-7} Pa or lower during analysis and the size of the analyzed area was 500 μm × 500 μm. Spectra were acquired with the angle between the direction of the emitted photoelectrons and the surface equal to 60°. The estimated analyzing depth of the used XPS set up was 8 to 10 nm. The high-resolution spectra were taken in the constant analyzer energy mode with a 200 eV for survey scan and a 50 eV pass energy for element scan, respectively. The value of 285.8 eV of the C 1 s core level was used for calibration of the energy scale. To curve fit the high-resolution C 1 s, S 2p, and O 1 s peaks, the deconvolution of C 1 s, S 2p, and O 1 s peaks was analyzed by the Thermo Avantage software. The peaks were deconvoluted using Gaussian–Lorentzian peak shapes (constrained between 80% and 100% Gaussian) and the full-width at half maximum (FWHM) of each line shape was constrained between 2.0 and 3.0 eV.

Results and Discussion

Electrical discharge behaviors during polymerization.—Figure 2 shows the spatial distribution of the plasma emission in the AP-plasma reactor during the polymerization with digital photographs (Fig. 2a) and ICCD images (Fig. 2b). The optical images indicated that the streamer discharge was maintained inside the guided tube, was strongest around the exposed bent area of the double V-shaped electrode, and was propagated from the electrode into space. The double V-shaped electrode configuration helped generate a large-area plasma medium. In the AP-plasma reactor with a pin-type electrode, the discharge is strongest at the electrode tip and spatially evenly distributed.[24] On the other hand, in this AP-plasma reactor, the bending region of the wire electrode where the discharge occurs is blunt and the bending edge is downward. Thus, the streamer propagation is formed in the shape of a canopy and the plasma medium is more widely distributed in the downward direction compared to that with the pin-type electrode.[27] Besides, since the double V-shaped electrode has the configuration of a cross-shaped wire electrode basically, it is possible to consider the two-dimensional spatial expansion of the discharge volume.

To use the AP-plasma generated from the bare wire electrode for polymerization, the distance between the powered electrode and the substrate (D) is significant for the growth of PTh thin film, and the discharge behaviors during plasma polymerization were investigated by adjusting D. It is observed that the streamer propagation occurred at the bent end of the electrode and the plasma medium is diffused inside the reactor due to being filled with the discharge gas.[28–32] The plasma intensity in the AP-plasma reactor increases as D reduces, as shown in Fig. 2. For a 17-mm D, the plasma generated from the electrode is in direct contact with the substrate during the AP-plasma polymerization, (Fig. 2b), term as the "plasma coupling mode" and the direct contact of the generated plasma with the substrate could damage its surface or change the properties of the deposited polymer film.[23–25] Because positioning the electrode as close to the substrate as possible under the plasma conditions where the plasma coupling mode does not occur is advantageous for the rapid growth of the polymer film while ensuring discharge stability and uniformity,[9] D was determined to be 22 mm in the formation of polymer films for ex situ and in situ I_2 doping tests.

To investigate the electrical behavior of the AP-plasma reactor, the applied voltage, discharge current, and optical emissions were measured as functions of time, and the results are presented in Fig. 3. The driven voltage maintained a steady sinusoidal waveform during the rise and fall of the discharge. The discharge current was obtained by subtracting the current measured while the driving voltage was applied in the absence of Ar gas (the displacement current), from the total current plotted on the digital oscilloscope when plasma was generated. As indicated in the figure, the discharge current occurs for both negative and positive applied voltages, indicating that plasma discharge occurs continuously throughout the cycle. The temporal behavior of the optical emission was measured near the bent area of the double V-shaped electrode in the AP-plasma reactor. The optical emission is detected only in the rising slope of the voltage waveform but periodically stable, indicating a streamer propagation generated when the powered electrode is an anode.

Morphological and chemical properties of PTh nanostructure.—The SEM images showing the surface morphology of the PTh nanostructured film synthesized with the proposed AP-plasma reactor for 10 min with the same magnification for non-doped (pure) and I_2-doped PTh films are shown in Fig. 4. The properties of the synthesized conducting polymers are controlled by combining several experimental conditions, including the argon gas flow, monomer vapor, doping method, deposition time, and distance between the substrate and electrode. Figure 4 shows the surface and cross-sectional morphologies of PTh films synthesized in all cases (i.e., non-doped, ex situ, and in situ I_2-doped). The high-magnification surface images in Fig. 4a indicate that this growth pattern consisted of irregularly crosslinked nanoparticles with a porous network. TEM observation confirmed that the PTh nanoparticles are interconnected to form a multi-cross-linked network with a diameter in the range of 20–60 nm, indicating that PTh nanoparticles are successfully synthesized. (See Fig. S1 (available online at stacks.iop.org/JSS/11/064005/mmedia) in Supplementary Material). Relatively densely packed nanostructures is observed in both pure and ex situ I_2-doped PTh films. Conversely, in the in situ I_2-doped PTh, the grain size of the nanoparticles did not change significantly, but the spacing among the nanostructures is widened, showing a greater porosity in the PTh film. The cross-sectional images provide information on the film growth, i.e., the crosslinked nanoparticles are predominantly aligned in the vertical direction (Fig. 4b). With the introduction of iodine into the PTh molecule, both ex situ and in situ I_2-doped molecules shows a reduction in the film growth. The introduction of iodine into the PTh nanostructures after polymerization (i.e., ex situ doping method) reduces the PTh film thickness by approximately 20% due to the particle aggregation in the polymer nanostructured films common during ex situ I_2 doping.[21]

Adding sublimated I_2 during the AP-plasma polymerization (i.e., in situ doping method), the grown PTh film becomes thinner than the

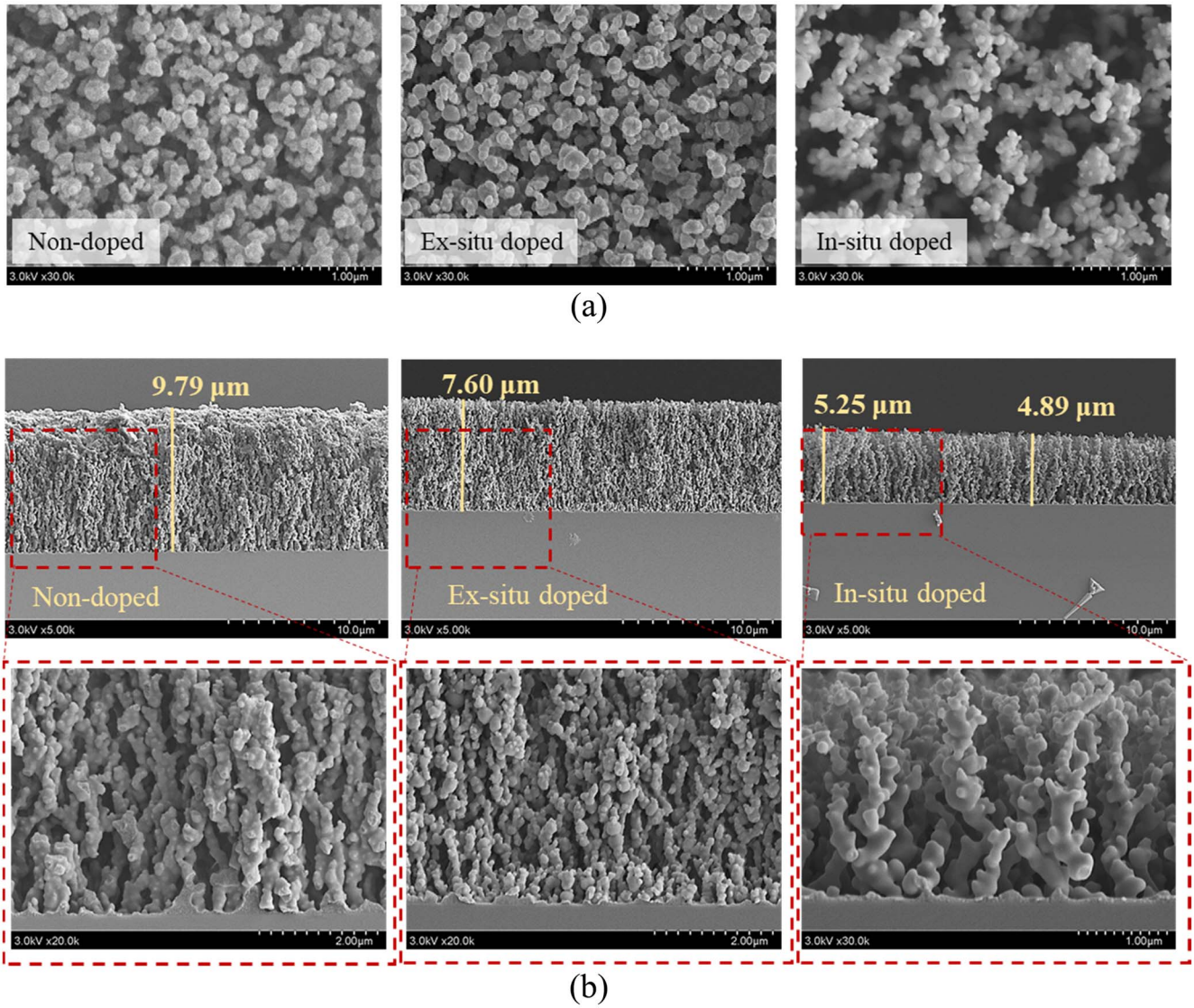

Figure 4. Field emission scanning electron microscopy (FE-SEM) images of the PTh nanostructure films synthesis on silicon substrate with the proposed AP-plasma reactor. (a) Plain view and (b) cross-section of non-doped (pure), in situ, and ex situ iodine-doped PTh nanostructure films.

pure PTh film, indicating that the I_2 molecules act as an impurity in the discharge, thereby reducing the reactivity of the monomeric species or polymer nanocomposite. The bottom images in Fig. 4b are the high-magnification cross-sectional images to identify the growth pattern of the PTh nanostructure. PTh nanostructures reveal the bumpy shapes of the crosslinked PTh nanoparticles with multiple protruding branches, with all PTh nanostructured films showing a vertical orientation. Notably, both the non-doped and ex situ I_2-doped PTh film show a closely packed nanostructured arrangement while the in situ case is loosely packed. Therefore, when I_2 molecules are introduced into the reactor chamber before polymerization for in situ doping, the density of the PTh nanostructure and the film thickness are simultaneously reduced in the synthesized PTh film.

The FTIR measurement was performed to investigate the molecular structure of the thiophene monomer and PTh films deposited on the silicon substrate in terms of non-doped and doped PTh films prepared by the in situ and ex situ I_2-doping processes. Fig. 5 reveals the characteristic peaks of the PTh films. These FTIR spectra of PTh films contain bands representing the C=C, C–H, and C–S bonds, corresponding to the thiophene monomer in Fig. 5.[33] Besides, peaks at 850 cm^{-1}, 1039 cm^{-1}, and 1155 cm^{-1} are associated with the C–S bond and in-plane deformation, respectively. The aliphatic characteristic peaks observed at 2927 cm^{-1} and 2972 cm^{-1} bands are attributed

Table II. Elemental concentration in atomic percentages of PTh films no-doped, ex situ, and in situ I_2 doping observed in XPS spectra in Fig. 6.

	Elemental concentration			
Sample	C 1s (at%)	S 2p (at%)	O 1s (at%)	I 3d (at%)
PTh without I_2 doping	63.9	19.0	17.1	0.0
PTh with ex situ I_2 doping	62.7	13.2	20.7	3.4
PTh with in situ I_2 doping	65.5	22.0	3.1	9.4

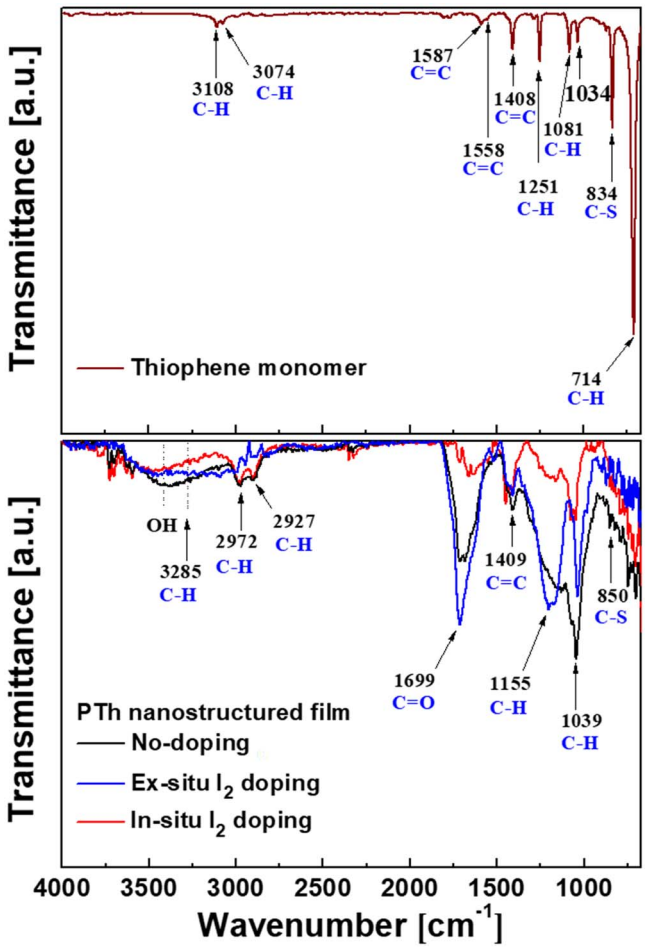

Figure 5. FTIR spectra of the thiophene liquid monomer and deposited PTh films on silicon substrate for non-doped, ex situ, and in situ iodine-doped cases.

to the C–H stretching vibration. Additionally, the peaks at 1409 cm^{-1} and 1699 cm^{-1} are assigned to the C=C asymmetric stretching vibration of the thiophene ring and C=O symmetric stretching, respectively.[9,19,20,33–36] These results confirm the presence of a thiophene ring in the PTh film structure. Herein, the absorption peak at C=O 1699 cm^{-1} confirms the inclusion of oxygen in the films during plasma deposition.[21] Furthermore, the FT-IR results show that the peaks at 1699 cm^{-1} (C=O) and 1039 cm^{-1} (C–H) bonds changed with the *ex-* and in situ I_2 doping processes. For the in situ I_2-doped PTh film, most spectra peaks significantly decrease due to the hydrogen absorption by the PTh film resulting from the I_2-doping, as shown in Fig. 5. Iodine radicals could be formed by the hemolytic dissociation of iodine. As iodine radicals could extract hydrogen atoms from the PTh structure, the bonding characteristics of the polymerized PTh films could be changed by the plasma process.[21,34] In addition, in case of the in situ I_2-doped PTh film, the decrease in the spectral intensity at 1699 cm^{-1} (C=O) is presumably due to the decrease in the relative amounts of surface reflection, originating from the film properties, such as surface roughness and particle size.[34]

Chemical composition of the PTh films obtained by FT-IR spectra is analyzed by comparing the XPS results. In Table II and Fig. 6a, the elemental concentration in atomic percentages and survey spectra identified from XPS are presented. The high resolution C 1 s, S 2p, O 1 s, and I 3d peaks are analyzed in detail, as presented in Figs. 6b–6e and S2 in the Supplementary Material. The peak assignments and envelope compositions of various C 1 s, S 2p, and O 1 s are summarized in Tables III–V, respectively. The XPS survey spectra in Fig. 6a show signals corresponding to C 1 s (285.5 eV), S 2 s (228.1 eV), S 2p (164.0 eV), O 1 s (532.1 eV), I $3d_{3/2}$ (631.6 eV), I $3d_{5/2}$ (620.1 eV), and I 4d (53.0 eV) electronic orbitals. Since the PTh films are in oxidized states due to synthesis under ambient air condition, the presence of O atoms in the PTh films can be expected, which is in agreement with the FT-IR data. The C 1 s peak can be divided into three distinctive component peaks (Figs. 6b, S2, and Table III) attributed to C–C, C=C, C–H bonds (284.7 eV), C–S bond (286.05 eV), and C–O bond (288.03 eV).[33,34] The S 2p peak can be split into three component peaks (Figs. 6c, S2, and Table IV) mainly contributed by aromatic sulfide (C–S–C, 164.35 eV), sulfoxide (C–SO–C, 165.55 eV), and sulfone ($C–SO_2–C$, 168.38 eV).[34,37] The O 1 s peak is also decomposed in three peaks (Figs. 6d, S2, and Table V). From the spectra of O 1 s, it can be seen that S-doped carbon displays the same oxygen species of O–C–O (532.76 eV) and O=C–O (533.99 eV). In addition, it also has a characteristic peak at 531.59 eV, which is attributed to the S-containing group S=O.[34,37,38] The XPS spectra exhibited by I 3d core of the I_2-doped PTh are shown in Fig. 6e, which shows the location of I $3d_{5/2}$ and I $3d_{3/2}$ peaks at the binding energy of 620.1 and 631.6 eV, respectively.[34,38,39]

Table III. Peak assignment (BE, eV) and envelope composition (%, total=100) of various C 1 s core level spectra of PTh films observed in XPS in Fig. 6.

	C 1s peaks assignment and envelope composition		
Sample	284.53 C–C, C–H, C=C	285.61 C–S	287.67 C–O
PTh without I_2 doping	40.2	47.6	12.2
PTh with ex situ I_2 doping	40.5	56.1	3.4
PTh with in situ I_2 doping	33.5	63.2	3.3

Table IV. Peak assignment and envelope composition of various S 2p core level spectra of PTh films observed in XPS in Fig. 6.

	S 2p peaks assignment and envelope composition		
Sample	164.86 C–S–C	166.18 C–SO–C	168.73 $C–SO_2–C$
PTh without I_2 doping	55.5	41.3	3.2
PTh with ex situ I_2 doping	61.0	37.1	1.9
PTh with in situ I_2 doping	50.7	47.5	1.8

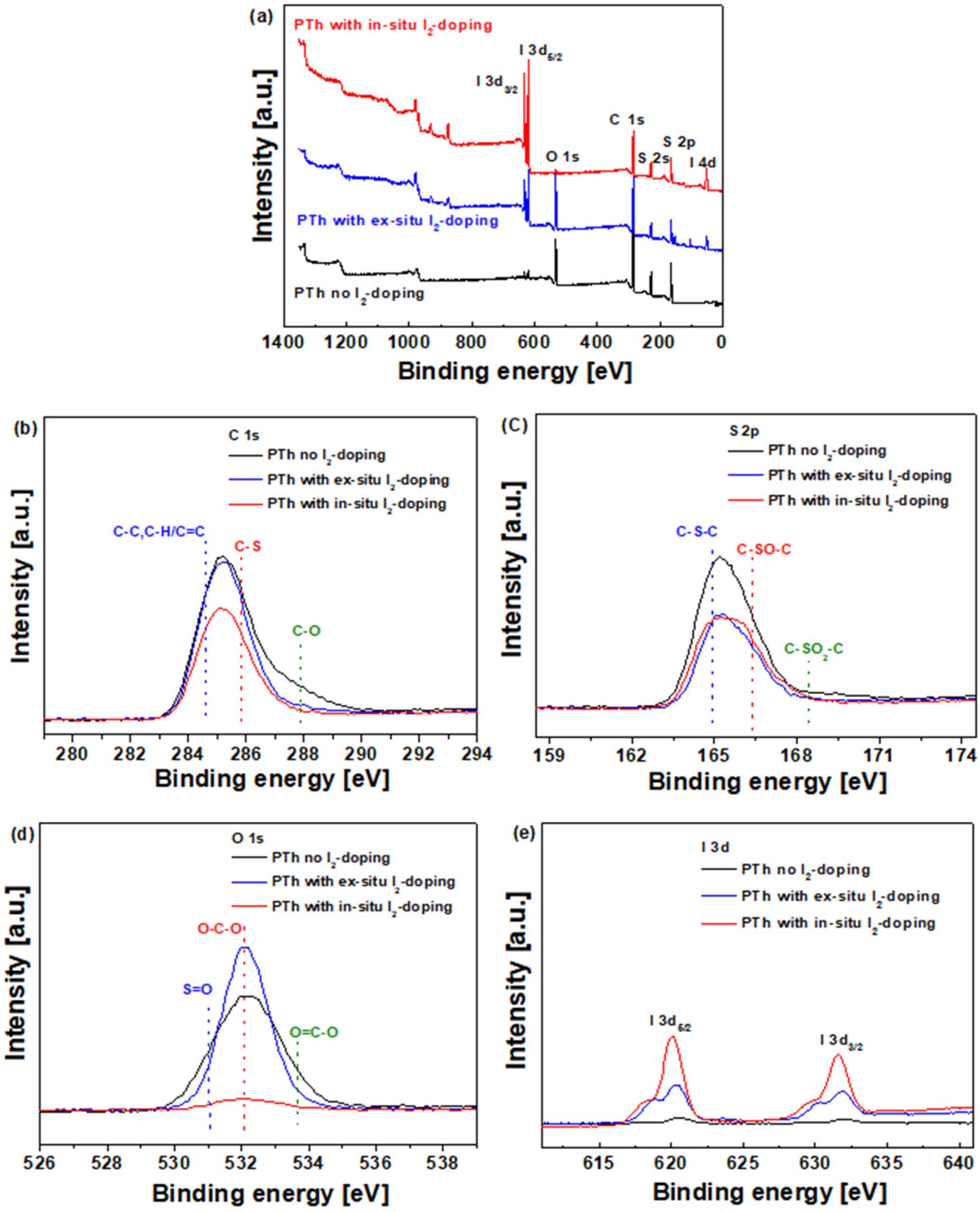

Figure 6. (a) XPS spectra of the plasma polymerized thiophene films without and with I_2 doping. High-resolution XPS spectra of (b) C 1 s, (c) S 2p, (d) O 1 s, and (e) I 3d of the no-doped, ex situ, and in situ iodine-doped PTh films.

After in situ I_2 doping, the carbons with oxidation, such as C–O and O–C–O, are remarkably decreased. The atomic percentage of C–C, C–H, and C=C bonds decreases from 40.2 to 33.5%, indicating some disruption to the conjugated framework of the films (Table III).[34,39] Whereas, S-containing groups with carbon and oxygen, such as C–S and C–SO–C increase when adopting the

Table V. Peak assignment and envelope composition of various O 1 s core level spectra of PTh films observed in XPS in Fig. 6.

	O 1s peaks assignment and envelope composition		
Sample	531.59 S=O	532.76 O–C–O	533.99 O=C–O
PTh without I_2 doping	21.5	65.2	13.0
PTh with ex situ I_2 doping	12.6	77.6	9.8
PTh with in situ I_2 doping	40.1	52.0	7.9

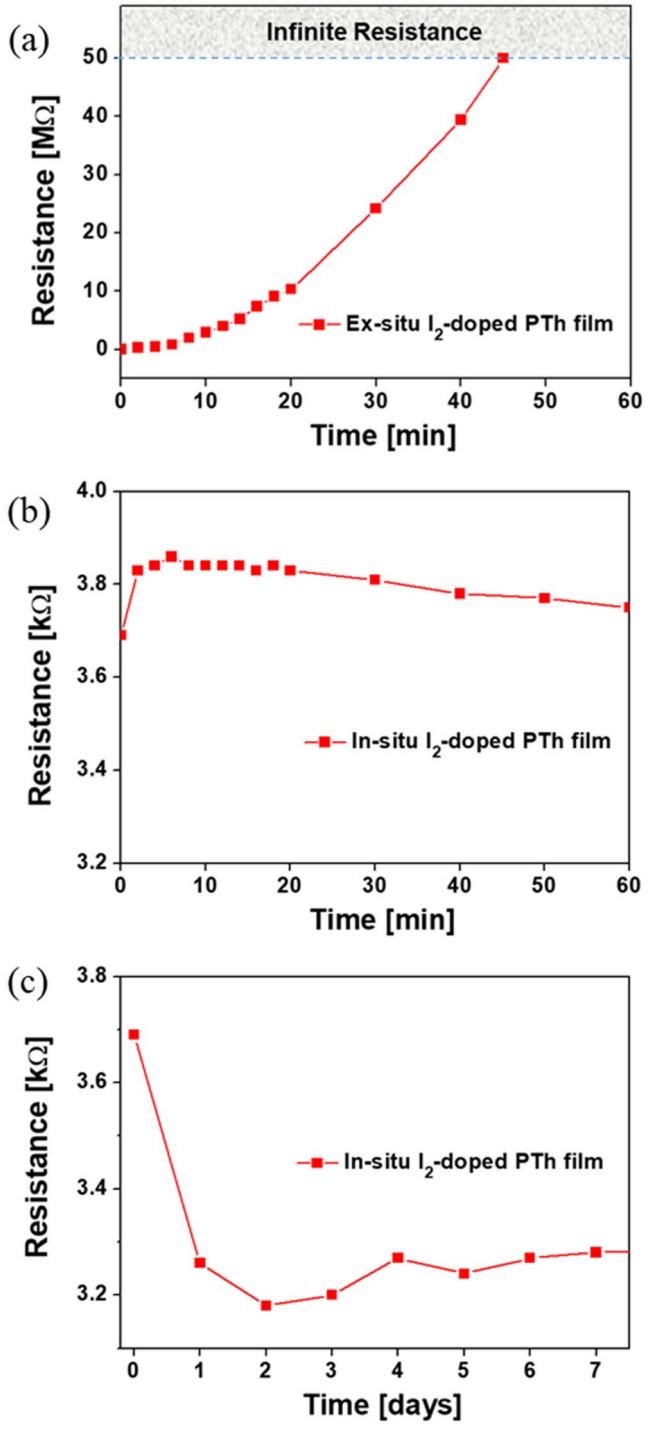

Figure 7. Comparison of the resistance variations in (a) ex situ and (b) in situ iodine-doped PTh films on interdigitated electrode (IDE) substrates for 1 h and (c) resistance variation of in situ iodine-doped PTh film for 7 d.

in situ I_2 doping (Tables III and IV). Total amounts of oxygen decrease strongly. In addition, since iodine could easily absorb hydrogen from materials, this reduced the C–H bond.[33,34]

Electrical property of iodine-doped PTh nanostructure.—To impart electrical properties to the synthesized PTh nanostructured film, PTh was doped by introducing I_2 molecule into it, either during (in situ doping) or after the PTh nanostructure synthesis (ex situ doping), as depicted in the experiment section. The resistance variation of the I_2-doped PTh film with time was measured using an IDE substrate consisting of a comb-binding array of gold electrodes. The measurement limit of the I_2-doped PTh film is 50 MΩ, and on exceeding this limit, it was considered infinity.

Figure 7a presents the variation in the resistance with time for the ex situ I_2-doped PTh nanostructured film on the IDE substrate. For the ex situ I_2-doped PTh film, the initial resistance was about 8.3 kΩ, and the resistance increases with the exposure time, rising to 38.35 MΩ in 40 min and reaching infinity (50 MΩ) within 45 min. The conductivity of the I_2-doped PTh film obtained by the ex situ method deteriorated rapidly over time, because the I_2 molecules did not participate in the polymerization process at all and additionally diffused to the PTh nanostructures by vacuum-sealing after polymerization. As a result, it is observed that the ex situ I_2-doped PTh film exhibits a disadvantage in that the electrical conductivity deteriorates with humidity. When this ex situ I_2-doped PTh film is left in the ambient air, the change in conductivity with time becomes a critical disadvantage as an electrical material, and its application to electronic devices is also limited because additional processes such as sealing or encapsulation is required.

Whereas, the in situ I_2-doped PTh nanostructures continued to undergo charge transfer by I_2 molecules during polymerization, thus resulting in relatively insensitive electrical properties into the external atmosphere. The initial resistance was around 3.7 kΩ, which increased to around 3.9 kΩ after 6 min of exposure time. The resistance did not remain constant but decreased very slowly to 3.7 kΩ after 60 min of exposure time, as represented in Fig. 7b. To ascertain the resistance stability of the in situ I_2-doped PTh nanostructured film, the resistance behavior was monitored and visualized for 7 d, as shown in Fig. 7c. The long-term monitoring of the resistance value shows a drop of about 450 Ω after a day and a highly stable resistance that did not change even by 0.1 kΩ for 7 days, with insignificant changes during storage under ambient conditions for 4 weeks. The experimental results confirm that it took one day for the resistance to stabilize. Nevertheless, the electrical resistance stabilizes and remains unchanged at a low value range of 3.2–3.3 kΩ. Although this resistor behavior is not ideally constant, the in situ I_2-doped PTh nanostructured film is a good resistor with the suitable resistance values. Therefore, the in situ I_2-doped PTh film exhibits very solid electrical properties in the ambient environment, and can be used in electronic devices, such as a transducer in gas sensors.

Conclusions

In this study, a new AP-plasma reactor with a double V-shaped bare electrode produced a stable discharge and secured the plasma polymerization medium for the PTh synthesis. The proposed

AP-plasma reactor also had the advantage of facile spatial expansion due to the common electrode with multiple wires. Plasma ignition occurred from the electrode part exposed to the mixed gas in the reactor chamber, and the plasma intensity increased as the distance between the electrode and substrate decreased. The resulting PTh nanostructured films were characterized for the nascent, ex situ, and in situ I_2-doped cases to determine their morphological, chemical, and electrical properties. The electrical resistance measurements confirmed that the in situ I_2-doped PTh film exhibited an excellent electrical conductivity without the electrical aging behavior. The new PTh films grown at room temperature using the proposed AP-plasma reactor can also offer versatile advantages as the electrodes and active layers for future displays and polymer gas sensors. Further studies on the change in the length and bending angle of tungsten wire exposed to plasma space will provide important experimental data for developing advanced AP-plasma polymerization techniques that can produce large-area and uniform polymer films using multiple common electrodes.

Acknowledgments

This study was supported by two National Research Foundation of Korea (NRF) grants funded by the Korean government (MOE) (No. 2020R1I1A3071693 and No. 2021R1I1A3049028) and the BK21 FOUR project funded by the Ministry of Education, Korea (4199990113966).

ORCID

Heung-Sik Tae https://orcid.org/0000-0002-4261-7581

References

1. C. Tendero, C. Tixier, P. Tristant, J. Desmaison, and P. Leprince, *Spectrochim. Acta - Part B At. Spectrosc.*, **61**, 2 (2006).
2. H. J. Jang, E. Y. Jung, T. Parsons, H.-S. Tae, and C.-S. Park, *Polymers*, **13**, 2267 (2021).
3. M. Laroussi and T. Akan, *Plasma Process. Polym.*, **4**, 777 (2007).
4. J. Friedrich, *Plasma Process. Polym.*, **8**, 783 (2011).
5. S. Asadollahi, J. Profili, M. Farzaneh, and L. Stafford, *Materials*, **12**, 219 (2019).
6. V. Mazánková et al., *Polymers*, **12**, 2679 (2020).
7. F. Moix, K. McKay, J. L. Walsh, and J. W. Bradley, *Plasma Process. Polym.*, **13**, 236 (2016).
8. G. Mertz et al., *Plasma Process. Polym.*, **15**, 1 (2018).
9. J. Y. Kim, H. J. Jang, G. T. Bae, C.-S. Park, E. Y. Jung, and H.-S. Tae, *Nanomaterials*, **12**, 32 (2022).
10. J. P. Borra, A. Valt, F. Arefi-Khonsari, and M. Tatoulian, *Plasma Process. Polym.*, **9**, 1104 (2012).
11. D. Hegemann, B. Nisol, S. Watson, and M. R. Wertheimer, *Plasma Chem. Plasma Process.*, **37**, 257 (2017).
12. M. Gerard, A. Chaubey, and B. D. Malhotra, *Biosens. Bioelectron.*, **17**, 345 (2002).
13. T. P. Kaloni, P. K. Giesbrecht, G. Schreckenbach, and M. S. Freund, *Chem. Mater.*, **29**, 10248 (2017).
14. J. Janata and M. Josowicz, *Nat. Mater.*, **2**, 19 (2003).
15. K. Namsheer and S. R. Chandra, *RSC Adv.*, **11**, 5659 (2021).
16. N. Ballav and M. Biswas, *Polym. Int.*, **53**, 198 (2004).
17. A. Husain, S. Ahmad, and F. Mohammad, *J. Sci.: Adv. Mater. Devices*, **5**, 84 (2020).
18. C. S. Park, C. Lee, and O. S. Kwon, *Polymers*, **8**, 249 (2016).
19. T. M. S. K. Pathiranage, D. S. Dissanayake, C. N. Niermann, Y. Ren, M. C. Biewer, and M. C. Stefan, *J. Polym. Sci., Part A: Polym. Chem.*, **55**, 3327 (2017).
20. H. Zhang, L. Hu, J. Tu, and S. Jiao, *Electrochim. Acta*, **120**, 122 (2014).
21. C.-S. Park, E. Y. Jung, D. H. Kim, D. Y. Kim, H. Lee, B. J. Shin, D. H. Lee, and H.-S. Tae, *Materials*, **10**, 1272 (2017).
22. C.-S. Park, D. Y. Kim, D. H. Kim, H.-K. Lee, B. J. Shin, and H.-S. Tae, *Appl. Phys. Lett.*, **110**, 033502 (2017).
23. D. H. Kim et al., *Mol. Cryst. Liq. Cryst.*, **663**, 108 (2018).
24. J. Y. Kim, S. Iqbal, H. J. Jang, E. Y. Jung, G. T. Bae, C.-S. Park, B. J. Shin, and H.-S. Tae, *Materials*, **14**, 1278 (2021).
25. D. H. Kim, C.-S. Park, E. Y. Jung, B. J. Shin, J. Y. Kim, G. T. Bae, H. J. Jang, B.-G. Cho, and H.-S. Tae, *Mol. Cryst. Liq. Cryst.*, **677**, 135 (2019).
26. P. Zhang, S. Zhang, F. Kong, C. Zhang, P. Dong, P. Yan, X. Cheng, K. K. Ostrikov, and T. Shao, *Surf. Coatings Technol.*, **387**, 125511 (2020).
27. H. S. Fricker, *Phys. Educ.*, **24**, 157 (1989).
28. E. Robert, T. Darny, S. Dozias, S. Iseni, and J. M. Pouvesle, *Phys. Plasmas*, **22**, 122007 (2015).
29. Y. Morabit, M. I. Hasan, R. D. Whalley, E. Robert, M. Modic, and J. L. Walsh, *Eur. Phys. J. D*, **75**, 32 (2021).
30. Z. Xiong and M. J. Kushner, *Plasma Sources Sci. Technol.*, **21**, 034001 (2012).
31. E. Robert, E. Barbosa, S. Dozias, M. Vandamme, C. Cachoncinlle, R. Viladrosa, and J. M. Pouvesle, *Plasma Process. Polym.*, **6**, 795 (2009).
32. T. Darny, J.-M. Pouvesle, J. Fontane, L. Joly, S. Dozias, and E. Robert, *Plasma Sources Sci. Technol.*, **26**, 105001 (2017).
33. T. Teslaru, I. Topala, M. Dobromir, V. Pohoata, L. Curecheriu, and N. Dumitrascu, *Mater. Chem. Phys.*, **169**, 120 (2016).
34. C.-S. Park, D. Y. Kim, E. Y. Jung, H. J. Jang, G. T. Bae, J. Y. Kim, B. J. Shin, H.-K. Lee, and H.-S. Tae, *Polymers*, **13**, 1783 (2021).
35. S. T. Navale, A. T. Mane, G. D. Khuspe, M. A. Chougule, and V. B. Patil, *Synth. Met.*, **195**, 228 (2014).
36. C. Rassie, R. A. Olowu, T. T. Waryo, L. Wilson, A. Williams, P. G. Baker, and E. I. Iwuoha, *Int. J. Electrochem. Sci.*, **6**, 1949 (2011).
37. H. Ji, T. Wang, Y. Liu, C. Lu, G. Yang, W. Ding, and W. Hou, *Chem. Commun.*, **52**, 12725 (2016).
38. M. Zhu, W. Zhang, Y. Li, L. Gai, J. Zhou, and W. Ma, *J. Mater. Chem. A*, **4**, 19060 (2016).
39. T. T. Kantzas, J. C. Byers, and O. A. Semenikhin, *J. Electrochem. Soc.*, **159**, H885 (2012).